Ocean Engineering 37 (2010) 1243–1252

Contents lists available at ScienceDirect

Ocean Engineering

journal homepage: www.elsevier.com/locate/oceaneng

Fatigue strength assessment of MARK-III type LNG cargo containment system

Myung Hyun Kim [a,*], Sang Min Lee [a], Jae Myung Lee [a], Byung Jae Noh [b], Wha Soo Kim [b]

[a] Department of Naval Architecture and Ocean Engineering, Pusan National University, 30 Jangjeon-dong, Geumjeong-gu, Busan 609-735, Republic of Korea
[b] Hull Initial Design Department, Hyundai Heavy Industries CO., LTD., Ulsan, Republic of Korea

ARTICLE INFO

Article history:
Received 7 August 2009
Accepted 13 May 2010
Available online 19 June 2010

Keywords:
Fatigue strength
Fatigue failure mode
Mark-III
Liquefied natural gas
Cargo containment system
Insulation system

ABSTRACT

The aim of this paper is to investigate the fatigue strength of the GTT Mark-III type LNG insulation system. The LNG insulation system consists of several composite layers with various connections; plywood, triplex, reinforced polyurethane foam and mastic. Consequently, the LNG insulation system may include mechanical failures such as cracks as well as delaminations within the layers due to sloshing impact loads and fatigue loadings. In addition, these failures may cause a significant decrease of structural integrity. In this study, a series of fatigue tests have been carried out for Mark-III type LNGC insulation systems at room temperature considering the effect of sloshing impact. The load levels have been determined based on the ultimate strength of reinforced polyurethane foam. The aim of the study is to investigate the typical failure characteristics of the MARK-III LNG insulation system and to obtain the S–N data under fatigue loading. A consolidated single S–N curve is obtained based on a systematic finite element procedure. Future use of the S–N data in fatigue analysis requires that the response analysis is carried out using a finite element model with the same mesh density and material properties. This study can be used as a fundamental study for the fatigue assessment of the LNGC insulation system as well as a design guideline.

1. Introduction

In recent years, liquefied natural gas (LNG) has been expected to play an increasingly important part in the global energy market. The consumption of LNG is increasing faster than other available energy resources that are known to be less environmentally friendly. With the increasing demand for LNG, the size of LNG carriers needs to increase rapidly, resulting in severe sloshing impact actions being encountered more often (Lee et al., 2006; Chun et al., in press; Lee et al., 2004). For the identification of sloshing impact loads inside LNG cargo holds, model tests with a scaled model or numerical analyses are typically performed (Bunnik and Huijsmans, 2009; Lee et al., 2007; Peric et al., 2009). In the design and construction of LNG carriers, dynamic failure of the LNG cargo containment system under fatigue loading due to sloshing impact actions is a key issue, among others, that must be resolved (Kim et al., 2006; Nam et al., 2005; MARINTEK, 2004). Raghavendran et al. (1988) performed a series of fatigue and fracture tests for aluminum–magnesium alloy used for LNG applications, particularly at a cryogenic temperature of −162 °C. Kaufman et al. (1980) carried out a structural integrity evaluation of a spherical aluminum storage tank using the fracture mechanics approach. Hurther et al. (1981) presented a methodology for fatigue analysis of Invar Gaz Transport type LNG carriers. However, all previous fatigue related studies did not consider the fatigue strength of the LNG insulation system. They considered the fatigue strength of aluminum or invar materials associated with LNG applications.

No significant accidents have been reported yet for conventional as-built LNG carriers. However, as the LNG market increases considerably, a new concept for LNG carriers having larger storage capacity as well as precise safety assessment schemes for a new containment system is required. The demand for LNG carriers with increased capacity requires further development of the design technology of LNG cargo tanks to meet safety requirements due to the larger size LNG tanks (Shin et al., 2006).

GTT Mark-III and NO96 types are the most common insulation systems employed for current LNG carriers. The NO96 type LNG cargo containment system consists of a grillage structure made of plywood and filled with perlite in order to maintain tightness and insulation. On the other hand, Mark-III type LNG cargo tanks consist of two layers of reinforced polyurethane foam divided by triplex material in order to configure the insulation system. In this study, the Mark-III type insulation system, which is increasingly used for LNG carriers, is considered for the evaluation of dynamic strength characteristics.

The cargo tanks of membrane type LNG carriers are comprised of insulation panels to maintain the cryogenic temperature (−163 °C) of liquefied natural gas. The surface of insulation

* Corresponding author. Tel.: +82 51 510 2486; fax: +82 51 512 8836.
E-mail address: kimm@pusan.ac.kr (M.H. Kim).

0029-8018/$ - see front matter © 2010 Elsevier Ltd. All rights reserved.
doi:10.1016/j.oceaneng.2010.05.004

panels is covered with a thin stainless steel layer of 1.2 mm thickness that has corrugations to absorb sloshing impact loads and thermal deformations. This stainless steel layer is called a membrane panel or the first barrier. Inside the membrane panel is two-layered reinforced polyurethane foam (R-PUF) with triplex. Triplex is embedded into the polyurethane foam to obtain sealing from gas leakage. Thus this component is called the secondary barrier. This insulation panel undergoes fatigue loadings of extension–compression due to the loading–unloading of LNG cargoes, and therefore sufficient mechanical strengths at a low temperature as well as fatigue strength need to be guaranteed.

The aim of this study is to investigate the fatigue performance of R-PUF at the highly loaded regions around the mastic supports and the slit region on the R-PUF. One of the main challenges in this work is to generalize the test results for use in the case of other mastic support sizes and spacings. Therefore, mastic supports with different sizes have been adopted during the fatigue tests to compare the fatigue performance as illustrated in Fig. 1.

The fatigue tests are carried out at room temperature. In particular, the sloshing effects are considered as taking the stress ratio at $R=-10$. The load levels have been determined based on the ultimate limit strength (ULS) of reinforced polyurethane foam 12.2 bar (Lee et al., 2006).

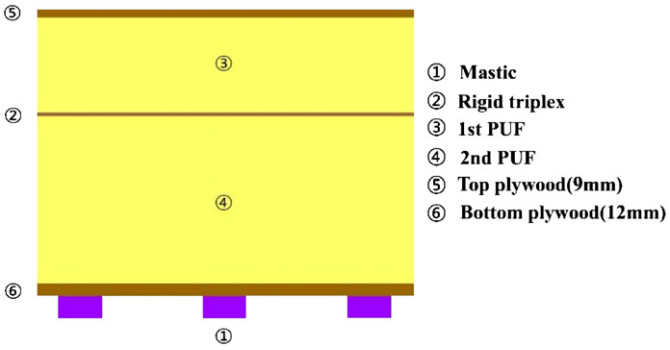

Fig. 2. Schematic of insulation panels.

Table 1
Dimension of the test specimen (unit: mm).

Height	271
Top plywood	12
1st PUF	89
Triplex	1
2nd PUF	160
Bottom plywood	9

2. Types of fatigue test specimens

Fatigue tests have been carried out using a unit section of the standard Mark-III insulation panels as illustrated in Fig. 2. The dimension matrix for the test specimens used in this study is summarized in Table 1. The overall dimensions of the test specimens are 340 mm by 340 mm with a thickness of 270 mm (Fig. 3).

There are three different types of specimens for the fatigue test. Type-A specimens have 40 mm wide mastic strips at the bottom, and Type-B specimens have 20 mm wide mastic strips. Identical distances between the mastic strips are maintained. Another type of test specimen, Type-C specimens, is devised for testing the fatigue strength at the slit areas as shown in Fig. 4. Note that Type-C specimens have no mastic support strips at the bottom. Type-C specimens were tested without a mastic support strip to evaluate the

Fig. 3. LNGC insulation panel.

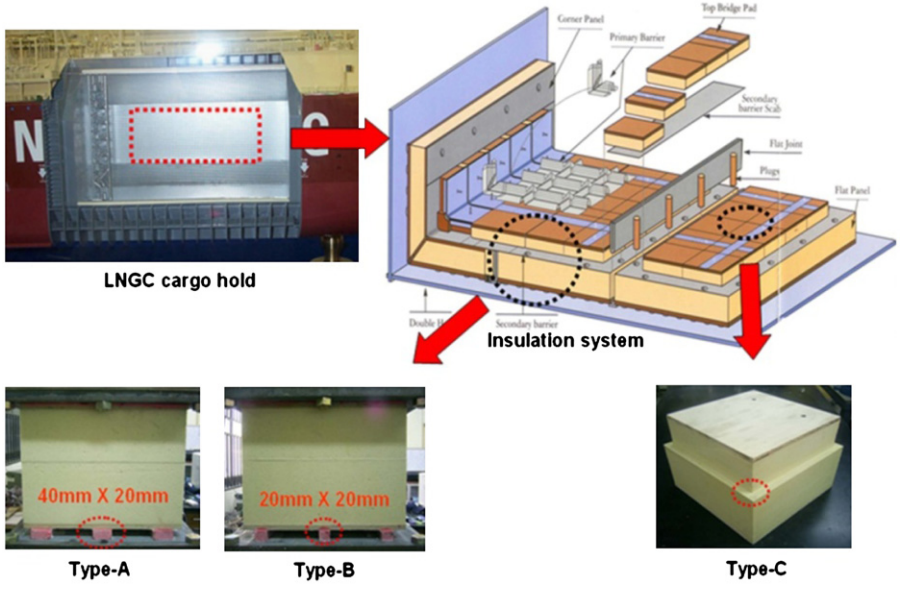

Fig. 1. Locations of test specimens in the LNG cargo hold.

a

Type-A

b

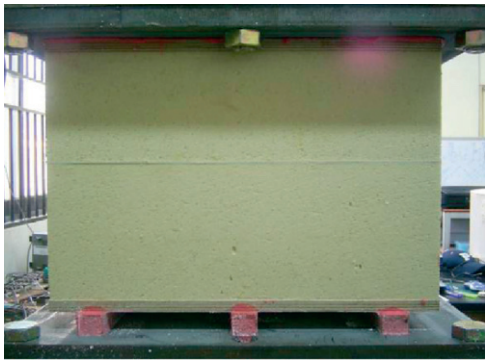

Type-B

c

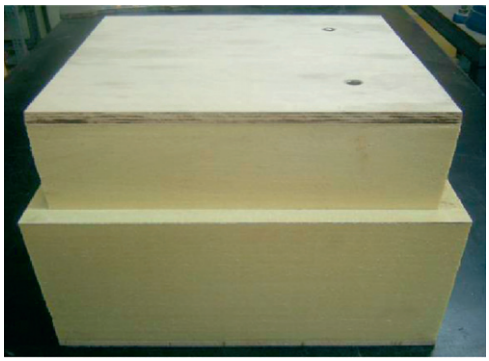

Type-C

Fig. 4. Test specimens for the fatigue strength test.

fatigue behavior in terms of the stress concentration induced by local geometry or the notch effect at slit locations. Fabricated mastic support strips have a rectangular section to obtain more reliable and consistent results from finite element analysis. The dimensions of the mastic and their location on the steel plate were maintained using Styrofoam sticks. A mixture of resin and hardener in accordance with shipyard practice was poured into the Styrofoam cast to obtain solid mastic support strips.

3. Experimental setup

3.1. Fabrication of test specimen

The fabrication procedure and the dimension of the test specimen considering the location of mastic are illustrated in Fig. 5. Once the mastic strips were fabricated, the mastic material used for test specimens as the mixture of resin and hardener in the weight fraction of 50:50 was fabricated on the steel plate. Original materials used for the mastic have been provided by Hyundai Heavy Industry, Inc. in order to obtain the closest possible proximity to shipyard practices. The special jig used for the arrangement of test specimens is as illustrated in Fig. 5. A mixture of resin and hardener was poured into the Styrofoam cast

Fig. 5. Fabrication procedure of mastics on test specimen.

to obtain solid mastic support strips. A square Styrofoam stick is used to make mastics in the desired dimensions. The rectangular section of mastic shapes has been considered to obtain more reliable results from finite element analysis. Both the top and bottom plywoods of the test specimens are attached between steel plates to apply tension during the cyclic loadings. A total of 6 steel plates are used for mastic fabrication during the air drying on the top side of the specimen, and the entire specimen was then left for approximately 24 h before completion. The procedure described so far is closely monitored according to shipyard practice. Improper procedures for the fabrication of mastic support strips resulted in early mastic failures during the fatigue test, such as the separation between the bottom plywood and the mastic support strip or the mastic softening. The problem was resolved by mixing resin and hardener in a double boiler condition as well as by following the accurate weight fraction of resin and hardener during mastic fabrication.

Standard Mark-III insulation panels have various geometric discontinuities such as slits and connection areas compared to other insulation panels (top bridge pad) around the triplex region. These defects will induce stress concentration due to the geometric discontinuities. Type-C specimens for Mark-III have considered geometric discontinuities at the triplex region as illustrated in Fig. 4. Type-C specimens have no mastic support strips in terms of evaluation of fatigue behavior at the geometric discontinuities.

3.2. Type-A specimens

Test specimens were fabricated as illustrated in Fig. 4(a). Fabricated mastic support strips have a 40 mm width and a 20 mm height. A relatively low stress distribution was observed at the regions around the mastic support strips when the mastic width increased.

3.3. Type-B specimens

Type-B test specimens were fabricated as illustrated in Fig. 4(b). Fabricated mastic support strips have a 20 mm width and a 20 mm height as the mastic size has been considered as a test parameter. A relatively higher stress distribution was observed at the regions around the mastic support strips. Mastic failure has been observed in some test specimens due to the decreased mastic width and improper procedure for the fabrication of the mastic support strip. In some cases, separation between the mastic and the bottom plywood has occurred due to the high stress at geometric discontinuity near the mastic adhesive region. However, failures due to the mastic separations were not used for the interpretation of S–N data.

3.4. Type-C specimens

Test specimens were considered for the fatigue strength assessment of geometric discontinuities at the slit areas near the triplex region. A standard Mark-III insulation system has slits in order to reduce stress caused by thermal deformation. The slit of an insulation system is narrow and deep from the upper plywood to near the triplex region, and is exposed to stress concentration. The type-C specimen was fabricated to consider the effect of geometric discontinuities using an artificial damage at the triplex region in order to find the crack propagation characteristics and the fatigue life of the Mark-III insulation system under fatigue load. Fatigue tests were carried out without using mastic support strips.

Fig. 6. Servo hydraulic fatigue test machine.

3.5. Fatigue test condition

The fatigue test machine used in this study is a servo-hydraulic fatigue test machine with the maximum load capacity of ± 20 ton (SAGINOMIYA®, Japan). The overall arrangement of the test equipment is shown in Fig. 6. The fatigue test machine is used for measuring the dynamic response of the insulation panel. The stress ratio R, the ratio of minimum stress over maximum stress, was set at -10, and the sinusoidal loads were applied at 1–3 Hz. The fatigue tests were tested until the final fracture (N_f). The final fracture is defined as the number of cycles when the test specimens are completely separated; while N_i is defined as the number of cycles until the first visible crack is observed in the test specimen. The test load levels were considered from the ultimate strength of reinforced polyurethane foam 12.2 bar under the load control condition.

4. Fatigue test results

4.1. Failure modes and characteristics

In this section, typical failure modes of the Mark-III insulation panel due to fatigue loadings are presented. As described earlier, all fatigue tests were carried out at the stress ratio of -10 and the cyclic frequency within the range 1–3 Hz.

Fatigue cracks are typically observed in most of the tests above the bottom plywood near the mastic support strips for Type-A and Type-B specimens. The other type of failure mode is the separation at the triplex region for Type-C specimens. Typical failure locations and characteristics for various load ranges are presented in Figs. 7–9. When Type-A and Type-B specimens were loaded near the elastic capacity of R-PUF, inelastic permanent deformations occurred in the foam above the support strips. In high load levels close to the ultimate strength of R-PUF, bottom plywood plates experienced fracture in the vicinity of mastic strips due to shear. In some cases, mastic strips of Type-B specimens were separated from the bottom plywood and/or softened during cyclic loadings due to improper preparation of mastics. Type-A specimens, however, had no such damage at adhesive regions above the mastic support strips due to the increased mastic width as well as the decreased stress at the region of the mastic strips.

As shown in Figs. 7 and 8, the typical failure location for Type-A and Type-B specimens was near the bottom plywood. The

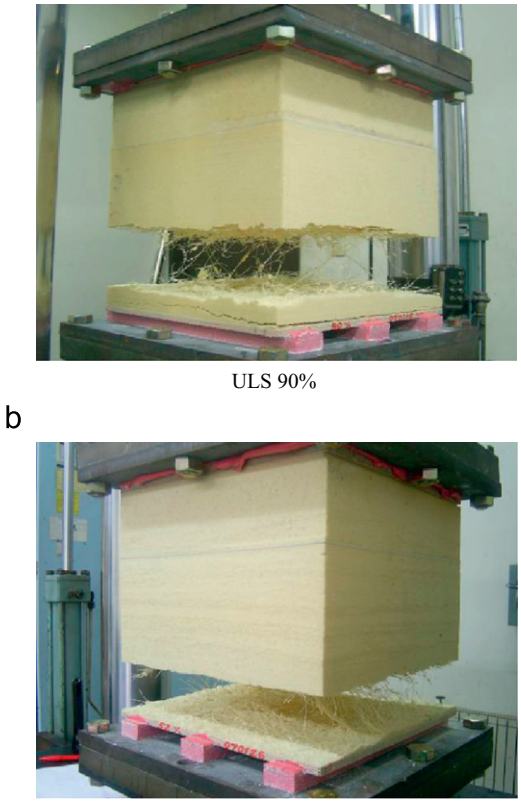

Fig. 7. Typical final failure modes of Type-A.

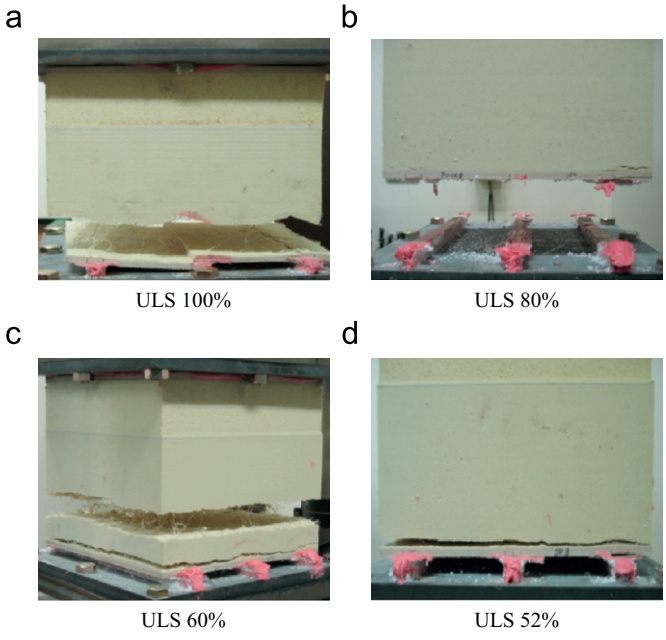

Fig. 8. Typical final failure modes of Type-B.

specimen shown in Fig. 7(a) was tested at the pressure range of 10.98 bar which corresponds to 90% of the ultimate strength of R-PUF. The initial crack was found at around 509 cycles in the vicinity of the bottom plywood. The final failure due to the complete fracture at the secondary R-PUF was observed at 4404 cycles. In the case of Type-B specimens, the bottom plywood

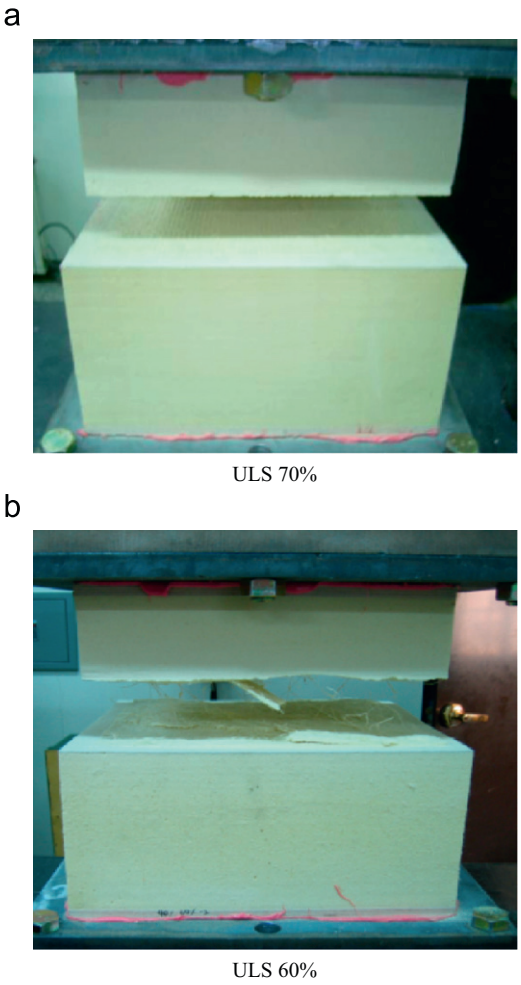

Fig. 9. Typical final failure mode of Type-C.

Table 2
Fatigue test result of Type-A specimens.

Spec. No.	ULS (%)/pressure (bar)	N_i (cycle)	N_f (cycle)	Failure mode
1	90/10.90	509	4,404	[a]
2	80/9.76	341	24,265	[a]
3	70/8.54	1360	33,289	[a]
4	65/7.93	12,800	94,760	[a]
5	65/7.93	27,370	179,680	[a]
6	60/7.32	20,900	333,340	[a]
7	52/6.35	43,160	814,850	[a]

[a] Separated between R-PUF and bottom plywood.

fractured due to shear when tested at the 12 bar as shown in Fig. 8(a). This is due to the increased stress concentration with a narrower mastic width (20 mm) than that of Type-A (40 mm) specimens as anticipated. Type-B specimens tested at lower load ranges experienced similar failure modes to those of Type-A specimens as shown in Fig. 8. Type-C specimens tested for the fatigue strength at the slit locations all failed at the above triplex regardless of load levels as illustrated in Fig. 9. This failure location is intended for the investigation of fatigue characteristics of the slit area because there are no other stress concentrated locations.

All fatigue test results such as the final fracture cycle, the first visible crack initiation cycle and the typical failure locations for each test specimen are summarized in Tables 2–4. Here N_i and N_f

Table 3
Fatigue test result of Type-B specimens.

Spec. No.	ULS (%)/pressure (bar)	N_i (cycle)	N_f (cycle)	Failure mode
1	100/12.20	–	770	[a]
2	100/12.20	–	430	[b]
3	90/10.98	182	388	[a]
4	90/10.98	153	359	[a]
5	80/9.76	207	1309	[a]
6	80/9.76	750	4232	[b]
7	70/8.54	1088	4085	[a]
8	70/8.54	2030	21,510	[a]
9	52/6.35	71,280	170,310	[a]
10	50/6.10	41,523	350,939	[a]

[a] Separated between R-PUF and bottom plywood.
[b] Separated between bottom plywood and mastics.

Table 4
Fatigue test result of Type-C specimens.

Spec. No.	ULS (%)/pressure (bar)	N_i (cycle)	N_f (cycle)	Failure mode
1	100/12.20	68	3705	[a]
2	100/12.20	163	6182	[a]
3	90/10.98	210	4185	[a]
4	90/10.98	183	6872	[a]
5	80/9.76	285	11,816	[a]
6	80/9.76	325	22,775	[a]
7	70/8.54	383	26,025	[a]
8	70/8.54	600	26,470	[a]
9	60/7.32	542	103,433	[a]
10	60/7.32	2982	239,307	[a]
11	50/6.10	4932	653,425	[a]

[a] Separated at the primary R-PUF above the triplex.

are defined as a fatigue crack initiation cycle and a fatigue failure cycle, respectively.

4.2. Crack propagation characteristics

Each specimen is tested until the final fracture. In other words, the final failure life of the LNG insulation system is defined as a complete separation of material due to sloshing impacts. However, such fractures are very unlikely in actual LNG ships due to the structural redundancy of the insulation system. Therefore, an attempt is made to consider the stiffness loss of the insulation system as an indication of fatigue failure. The stiffness curve is obtained by dividing the load range by the displacement range based on Eq. (1) using the following relationship:

$$Stiffness = \frac{Max.\ Load - Min.\ load}{Max.\ Disp - Min.\ Disp} \quad (1)$$

In order to obtain the stiffness curve, the EDX-1500A memory recorder/analyzer was employed to record the load and the displacement at every 990 cycles during each fatigue test. Normally, both load and displacement were recorded for 1 s at 100 Hz sampling rate. Fig. 10 illustrates typical stiffness measurements of two Type-A specimens with the cyclic loading ranges corresponding to 65% and 80% of ULS. Final failure cycles were 24,265 cycles for 65% ULS load range and 179,680 cycles for 65% ULS load ranges, respectively. Based on the stiffness measurement, it is noted that these cycles correspond to approximately a 20% stiffness decrease. This information could be useful for various failure definitions of LNG insulation systems including final fracture. In an actual situation, no complete fracture will occur because the sloshing impacts are mostly in compression. However, the loss of the stiffness of the insulation system could be used for the indication of structural failure of the insulation system.

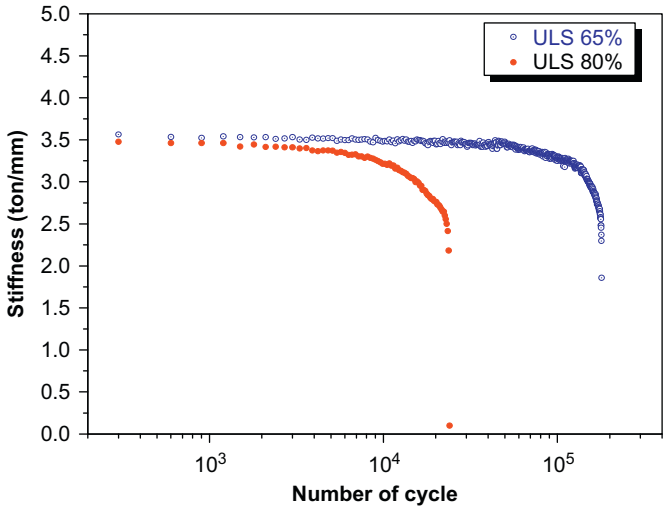

Fig. 10. Stiffness curve for specimen.

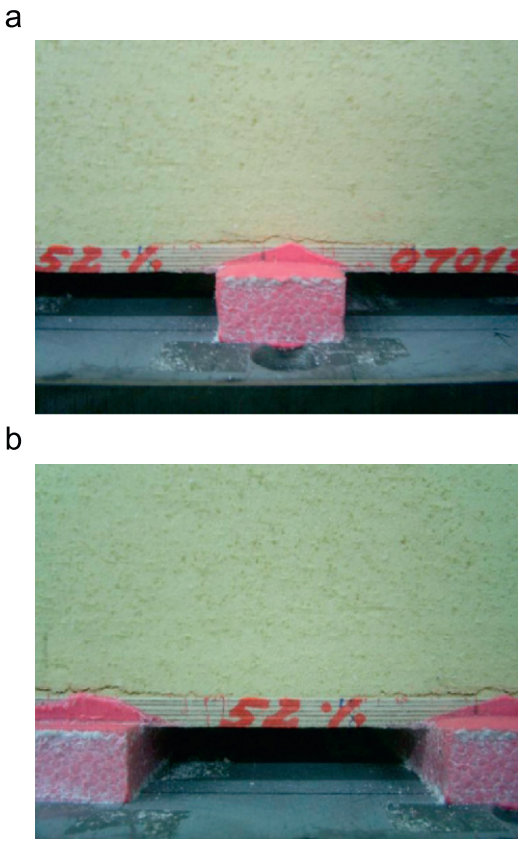

Fig. 11. Crack propagation near mastic support strips.

Most fatigue cracks were observed at stress concentration regions such as the location above the bottom plywood for Type-A and Type-B specimens and propagated horizontally as shown in Fig. 11. Typically cracks propagated slowly until reaching a specific load cycle. A significant part of the crack occurred and propagated between the bottom plywood and the secondary R-PUF. When cracks from the side surfaces of the specimen are all connected, the rate of crack propagation is accelerated. On the other hand, fatigue cracks of Type-C specimens have been observed at the four edges and propagated toward the inside of

the specimen. Typical failure of Type-C specimens occurred at the interface between the adhesive region of the triplex and the primary R-PUF as cracks propagated through the boundary. Also, the crack growth rate of Type-C was observed to be relatively faster than that of other types of specimens. This phenomenon is a key issue that needs further research in terms of safety evaluation of the secondary barrier of the LNG insulation system. Fig.12 shows the crack propagation behaviors in the case of different sizes of mastic width at the same fatigue loading rate. Type-A specimens have a longer propagation life than that of Type-B due to the increased mastic width.

4.3. S–N data correlation

This section presents the S–N data obtained from the fatigue test. The fatigue life of each specimen is presented in terms of the nominal pressure versus the failure cycles as illustrated in Fig. 13.

Type-A specimens have a longer fatigue life than that of Type-B due to the increased mastic width as shown in Fig. 13(a). Type-C specimens have a similar fatigue life to that of Type-A. It should be noted that the slopes of S–N data from all types of test specimens are alike. Fig. 13(b) compares the crack initiation life of test specimens considered in this study. It is observed that the crack initiation cycles of Type-C are comparatively faster than other types of specimens especially at low pressure. However, this does not necessarily indicate less fatigue life because it was easier to detect fatigue cracks at an early stage in the case of Type-C.

The S–N curves of Type-A and Type-B specimens from this study are compared with the experimental result of DNV (DNV, 2003) for a comparison of crack initiation life as illustrated in Fig. 14. There is a slight difference in the slope of the fitted line. Considering the difference in test specimens and test conditions, however, it is considered that the results are in good agreement. Note that DNV used test specimens cut from a Mark-III insulation panel and fitted with 25 mm width plywood support strips as a

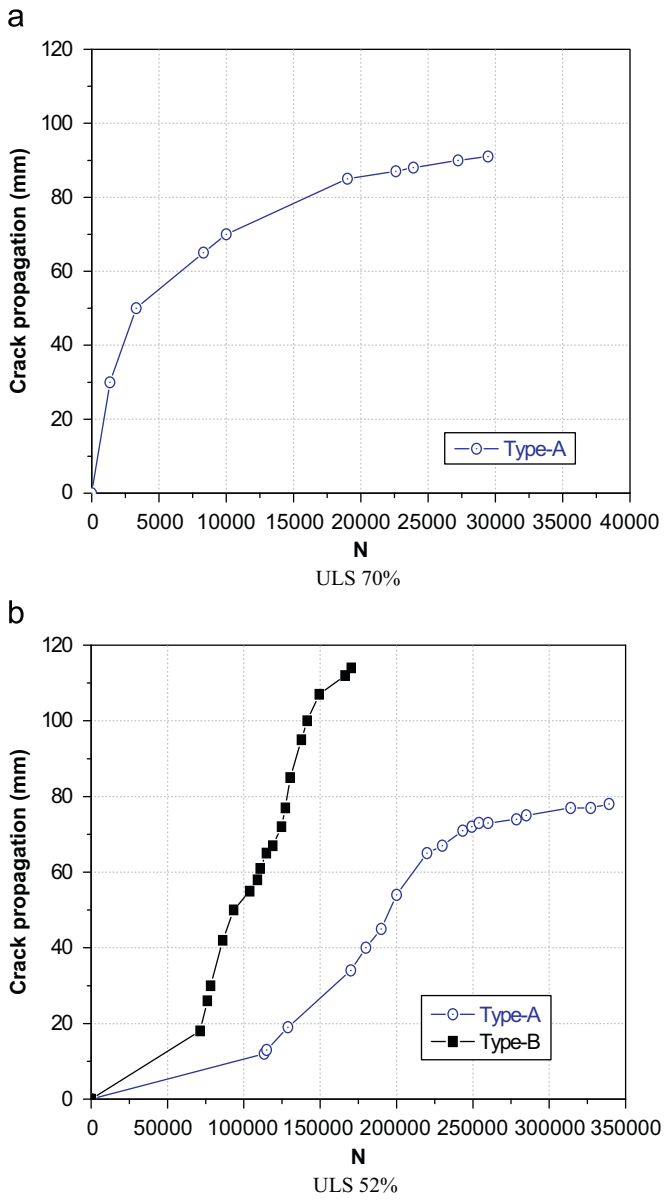

Fig. 12. Crack propagation at center mastic support: (a) ULS 70% and (b) ULS 52%.

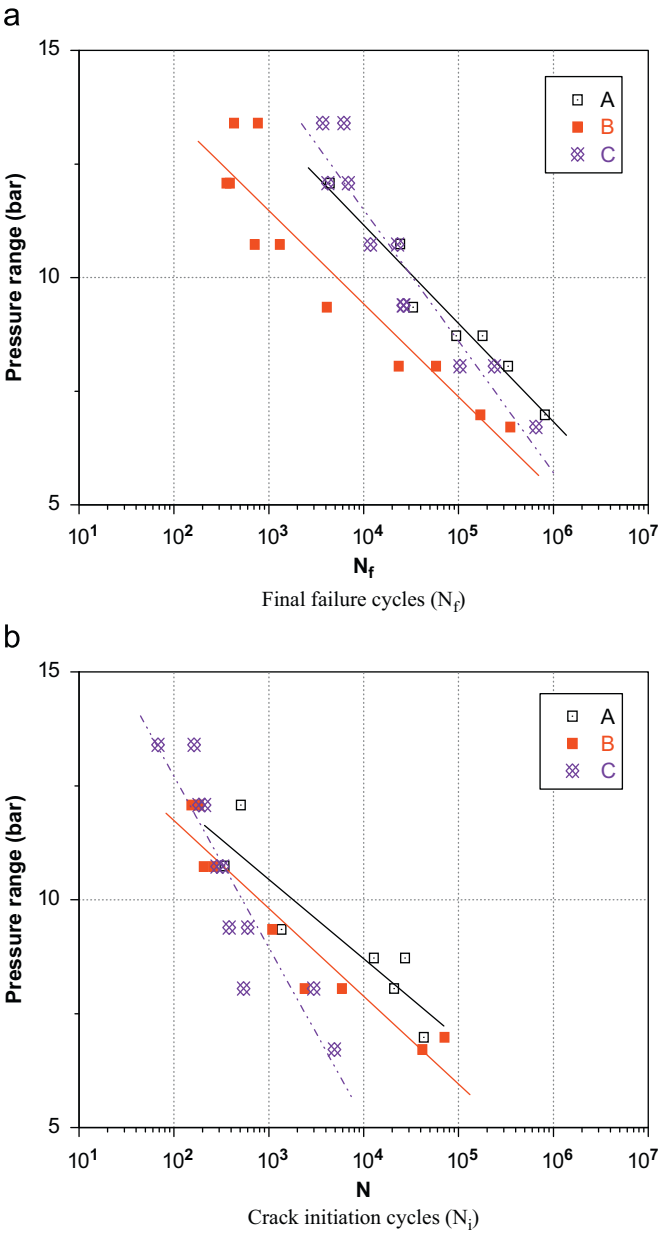

Fig. 13. Comparison of fatigue life in terms of applied pressure range: (a) final failure cycles (N_f) and (b) crack initiation cycles (N_i).

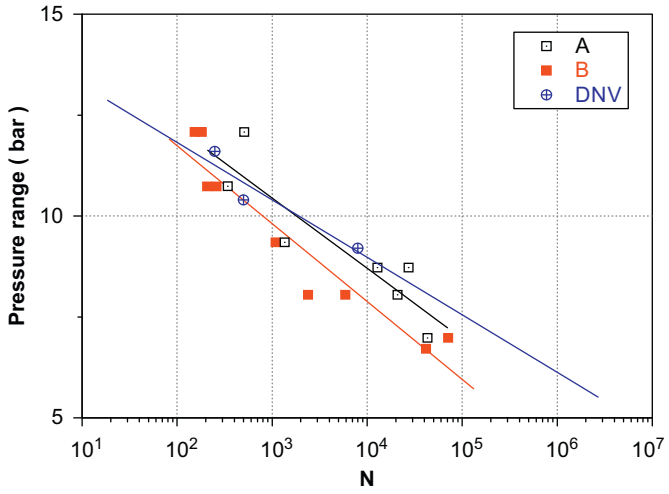

Fig. 14. Comparison of crack initiation life.

substitute for mastic. The stress ratio (R) was 0.01, and only three specimens were tested (DNV, 2003).

5. Finite element analysis

The fatigue test result in terms of the S–N curve is represented by local stresses at the critical material locations obtained by finite element analysis. The stress is calculated at fatigue failure locations observed during each test. A commercial finite element analysis code, MSC Nastran®, is used for the interpretation of the results of this study.

A specimen with dimensions of 340 mm by 340 mm and the thickness of 271 mm is considered for the numerical investigation. The orthotropic reinforced polyurethane foam material property was considered as illustrated in Table 5.

A convergence test was carried out with respect to various element sizes for the selection of the proper element size as shown in Fig. 15(b). The element sizes used in Fig. 15 are summarized in Table 6. As shown in Fig. 15(a), element size has a significant influence on the computed stress values, particularly at the failure location around mastic support strips. Fig. 15(b) compares the finite element models with different mesh densities in the vicinity of mastic strips. Later the element size of 20 mm × 20 mm mastic strips (Model-4 in Table 6.), is proposed based on the consistency for the interpretation of the S–N data.

Maximum element stresses in the thickness direction corresponding to the failure locations are later used as the local stresses in the S–N curve. In the case of Type-A and Type-B specimens, the local stress values calculated above the mastic strips are considered. The local stress of Type-C has been calculated on the top of the triplex layer at four corners. Stress components in the vertical direction obtained from FEA are used for each specimen type using isotropic and orthotropic material properties for each layer.

The fatigue test result is presented in terms of the S–N curve using the local stresses obtained from FEA and fatigue test results as shown in Fig. 16. The local stress was taken as the stress component in the thickness direction with the proposed element size of 20 mm × 20 mm mastic strips. The stress values calculated at the locations corresponding to experimentally identified failure locations are used. By using the proposed element size, a consistent fatigue design is possible with good accuracy in a reasonable computational time.

Table 5
Material properties of MARK-III insulation system.

	Plywood	PUF	Triplex	Mastic
E_n	8900	142	13,133	2934
E_s	7500	142	–	–
E_t	520	84	–	–
υ_{ns}	0.17	0.24	0.3	0.3
υ_{nt}	0.17	0.18	–	–
υ_{st}	0.17	0.18	–	–
G_{ns}	196	12.2	–	–
G_{nt}	196	12.2	–	–
G_{st}	196	12.2	–	–

E, G and υ indicate Young's modulus, shear modulus and Poisson ratio, respectively.
All units are MPa except for Poisson ratio.

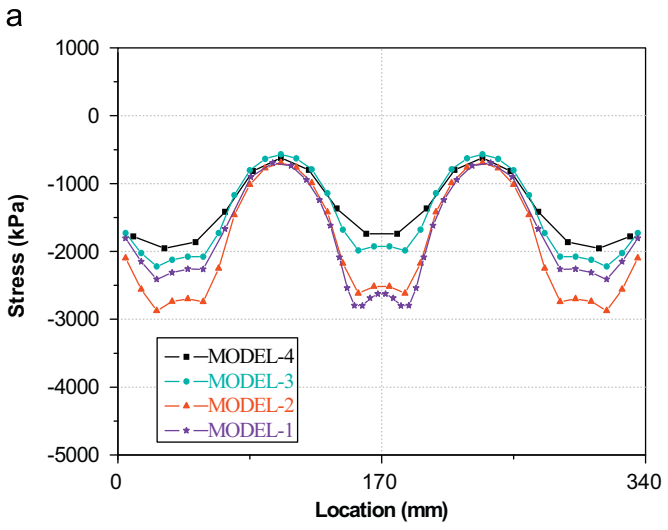

Stress distribution in X direction

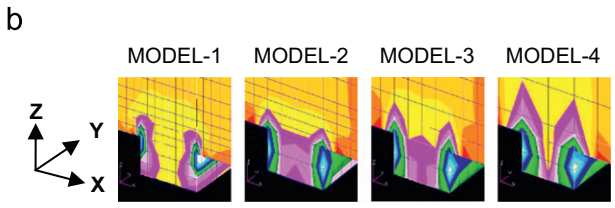

FE models for different mesh density

Fig. 15. Convergence test.

Table 6
Element size for convergence test.

Dimension (mm)	MODEL-1	MODEL-2	MODEL-3	MODEL-4
X-direction	5	10	10	20
Z-direction				
R-PUF	4	5	10	20
Plywood	4.5	4.5	9	9
Mastic	6.7	10	10	10

Fig. 16 presents the S–N data using the local stress calculated by FEA and the failure cycles obtained from the fatigue tests. A single consolidated S–N curve is found based on stress values calculated by FEA using the element stress obtained by 20 mm × 20 mm at the failure location as illustrated in Fig. 16.

It is important to note that the single curve includes all test data for three different specimen types. When fatigue life is

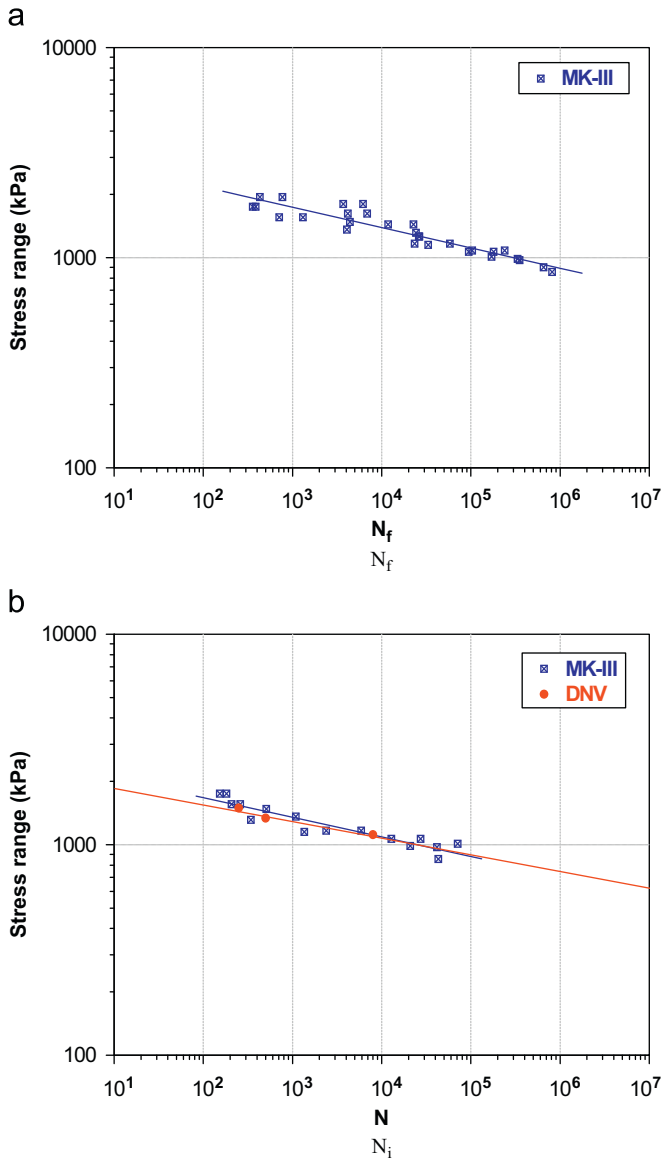

Fig. 16. A single consolidated S–N curve using a local stress at the corresponding failure locations: (a) final failure cycles (N_f) and (b) crack initiation cycles (N_i).

presented in terms of pressure, Type-B specimens appear to have the lowest fatigue strength. However, it can be observed that the fatigue strength for all fatigue vulnerable locations such as near the mastic strips and the slits between the primary and the secondary barriers in the LNG insulation system can be represented with the single consolidated S–N curve. This could be used as a fatigue strength assessment guideline for an LNG insulation system based on the finite element analysis technique with a sufficient safety for repeated sloshing impact loads. Fig. 16(b) shows the fatigue crack initiation cycles in terms of the local stress values calculated by the finite element method. It can be seen that the fatigue crack initiation cycles also consolidates into a single line. Moreover, it is found that the result appears to agree with the test results of DNV with good accuracy.

6. Summary

In this study, fatigue tests of the Mark-III type insulation system for three different locations have been carried out at room temperature. The sloshing impact loading condition is considered, taking the fatigue stress ratio as -10. The load levels have been determined based on the ultimate strength of reinforced polyurethane foam 12.2 bar. A total of 28 test specimens of 3 different types are used for the fatigue tests. The fatigue life as well as fatigue failure characteristics of the LNG insulation system are investigated. In addition, a fatigue design guideline based on the finite element analysis technique is proposed for the consistent fatigue assessment of the LNGC insulation system.

The major issues investigated in this study are summarized as follows:

- Three different types of specimens were designed and tested for the fatigue strength assessment of the MARK-III type insulation system of LNG carriers.
- Typical failure modes of Mark-III insulation panel were observed during fatigue tests. These are the fatigue cracks above the bottom plywood near mastic support strips. Other failures observed were mastic failures by mastic softening, separations between the bottom plywood and the PUF, and separations between the PUF on the triplex.
- For the fatigue design of the LNG insulation system using finite element analysis, the mastic strip with rectangular section has been considered to obtain reliable and consistent results. Based on the nominal stress, Type-A exhibits better fatigue life than that of Type-B specimens, due to an increased width of the mastic support strip.
- A series of FEA tests was performed in order to identify the design S–N curve based on the proper stress at failure locations. A consolidated single S–N curve that includes all test data is proposed based on element stress obtained by 20 mm × 20 mm element size at corresponding failure locations.

Acknowledgements

This research is sponsored by the Hyundai Heavy Industry, Inc. and Advanced Ship Engineering Research Center of Korea Science & Engineering foundation.

References

Bunnik, T., Huijsmans, R., 2009. Large-scale LNG sloshing model tests. International Journal of Offshore and Polar Engineering 19 (1), 8–14.

Chun, M.S., Kim, M.H., Kim, W.S., Kim, S.H., Lee, J.M. Experimental investigation on the impact behavior of membrane type LNG carrier insulation system, Journal of Loss Prevention in the Process Industries 22, 901–907.

Det Norske Veritas, 2003, Fatigue testing and analyses of the Mark III containment system for LNG, *JIP Report* (NO. 205-0218).

Hurther, M., Benoit, F., Poudret, J., 1981. Fatigue analysis method for LNG membrane tank details. In: Extreme Loads Response Symposium, Society of Naval Architecture and Marine Engineers, Arlington, USA, pp.89–100.

Kaufman, J.G., Bucci, R.J., Kelsey, R.A., 1980. Fracture-mechanics aspects of the structural integrity technology of spherical aluminum containment vessels for LNG tankers. Journal of Engineering Materials and Technology—Transactions of the ASME 102 (3), 303–314.

Kim, M.H., Kim, D.H., Kang, S.W., Lee, J.M., 2006. An Interlaminar strain measurement for insulation panels of LNG carriers. Strain An International Journal for Experimental Mechanics 42 (2), 97–106.

Lee, D.H., Kim, M.H., Kwon, S.H., Kim, J.H., Lee, Y.B., 2007. A parametric sensitivity study on LNG tank sloshing loads by numerical simulations. Ocean Engineering 34 (1), 3–9.

Lee, H., Kim, J.W., Hwang, C., 2004. Dynamic strength analysis for membrane type LNG containment system due to sloshing impact load. In: Proceedings of the International Conference on Design and Operation of Gas Carriers. London, UK.

Lee, J.M., Paik, J.K., Kim, M.H., Yoon, J.W., Choe, I.H., Kim, W.S., Noh, B.J., 2006. Strength of membrane type LNG cargo containment system under sloshing impact. In: World Maritime Technology Conference, London, UK.

MARINTEK, 2004. Sloshing test of 138k/4 tanks LNG ship with partial filling.

Nam, S.K., Kim, W.S., Noh, B.J., Shin, H.C., Park, I.H., Kim, D.E., Rashed, S., 2005. Structural response of membrane tanks to sloshing load in a MARK III type LNG carrier. In: Proceedings of the 19th Asian Technical Exchange and Advisory Meeting on Marine Structures, Singapore.

Peric, M., Zorn, T., Moctar, O., Schellin, T.E., Kim, Y.S., 2009. Simulation of sloshing in LNG-Tanks. ASME Journal of Offshore Mechanics and Arctic Engineering 131 (3), 117–128.

Raghavendran, N.S., Fourney, M.E., Lawrence, F.V., 1988. Fatigue-fracture behavior of 5083-0 aluminum magnesium alloy for LNG applications. Engineering Fracture Mechanics 29 (6), 647–662.

Shin, Y.S., Kim, J.W., Wang, B., 2006. First principle-based analysis procedure for strength assessment of membrane-type LNG containment system due to sloshing impact. In: World Maritime Technology Conference, London, UK.